

## Airborne stratospheric ITCIMS measurements of SO<sub>2</sub>, HCl, and HNO<sub>3</sub> in the aged plume of volcano Kasatochi

T. Jurkat,<sup>1</sup> C. Voigt,<sup>1,2</sup> F. Arnold,<sup>1,3</sup> H. Schlager,<sup>1</sup> H. Aufmhoff,<sup>1,3</sup> J. Schmale,<sup>4</sup> J. Schneider,<sup>4</sup> M. Lichtenstern,<sup>1</sup> and A. Dörnbrack<sup>1</sup>

Received 20 January 2010; revised 30 June 2010; accepted 2 July 2010; published 9 November 2010.

[1] Major explosive volcanic eruptions inject gases and ash particles into the stratosphere, resulting in significant impacts on ozone and climate. Here we report on fast and sensitive in situ measurements of sulfur dioxide (SO<sub>2</sub>), hydrochloric acid (HCl), and nitric acid (HNO<sub>3</sub>) in an aged stratospheric plume of volcanic origin made by an ion trap chemical ionization mass spectrometer (ITCIMS) aboard the research aircraft Falcon. Other instruments on the Falcon measured reactive nitrogen (NO<sub>y</sub>), carbon monoxide (CO), and ozone (O<sub>3</sub>) as well as the aerosol composition. The plume most likely originated from the 7–8 August 2008 eruption of the Aleutian volcano Kasatochi and almost 3 months later, on 31 October 2008, was encountered by the aircraft during two missions over Europe at altitudes between 7000 and 11,600 m. Within the plume, SO<sub>2</sub> mixing ratios of up to 0.51 ppbv were about a factor of 10 higher than in the background stratosphere (0.02–0.055 ppbv). The molar ratios HCl/O<sub>3</sub> and HNO<sub>3</sub>/NO<sub>y</sub> tended to be elevated by up to 19%, and HNO<sub>3</sub>/O<sub>3</sub> also showed a substantial enhancement inside the plume. From our measurements we infer an upper limit of the e-folding lifetime of 62 days for SO<sub>2</sub> conversion in the stratosphere, indicating that approximately 25% of the volcanic SO<sub>2</sub> had not yet experienced OH-induced conversion to sulfuric acid. Our measurements contribute to a better understanding of the formation of volcanic aerosol and of heterogeneous reactions taking place on these particles in the lower stratosphere.

**Citation:** Jurkat, T., C. Voigt, F. Arnold, H. Schlager, H. Aufmhoff, J. Schmale, J. Schneider, M. Lichtenstern, and A. Dörnbrack (2010), Airborne stratospheric ITCIMS measurements of SO<sub>2</sub>, HCl, and HNO<sub>3</sub> in the aged plume of volcano Kasatochi, *J. Geophys. Res.*, 115, D00L17, doi:10.1029/2010JD013890.

### 1. Introduction

[2] Volcanoes emit large amounts of sulfur and chlorine. Sulfur in volcanic gases released to the atmosphere is usually thought to be mostly in the form of SO<sub>2</sub>. Chlorine is emitted mostly as gaseous HCl and, to a smaller part, also as NaCl aerosol particles. For example, during the major explosive eruption of volcano Mount Pinatubo in 1991, the emitted masses were approximately 20 Mt SO<sub>2</sub> and 4.5 Mt HCl [McCormick *et al.*, 1995]. Hence the molar emission ratio of HCl to SO<sub>2</sub> was about 0.4. Explosive eruptions often emplace SO<sub>2</sub> into the stratosphere. There volcanic SO<sub>2</sub> undergoes photochemical conversion to gaseous sulfuric acid (GSA) [Arnold and Bührke, 1983; Stockwell and Calvert, 1983]. The conversion mechanism was later confirmed in laboratory

experiments by Reiner and Arnold [1993, 1994]. In turn, GSA experiences rapid conversion to sulfuric acid particles (SAP). First measurements of sulfuric acid in stratospheric SAP have been made by Arnold *et al.* [1998]. SAP influence ozone and other trace gases and global climate [Solomon *et al.*, 1998; World Meteorological Organization, 2007]. The NO<sub>x</sub> conversion to HNO<sub>3</sub> via SAP-catalyzed N<sub>2</sub>O<sub>5</sub> hydrolysis [Hanson and Ravishankara, 1991] has additionally an important influence on the trace gas distribution. This effect was demonstrated by the detection of a marked increase of HNO<sub>3</sub> in the aged stratospheric plume of the 1982 Mt El Chichón eruption at 25 to 26 km altitude [Arnold *et al.*, 1990]. By absorption of terrestrial infrared radiation SAP induce stratospheric warming and by scattering incoming sunlight back to space they increase the planetary albedo, which leads to global cooling of the planetary surface. Downward mixing of stratospheric sulfate aerosol particles into the troposphere may also have an indirect climate effect. In the troposphere such particles may act as condensation nuclei for cloud droplets. An analogy consideration of this sulfur cooling effect of volcanic eruptions has led to the idea of climate engineering by injecting anthropogenic sulfur gases into the stratosphere [Crutzen, 2006; Caldeira and Wood, 2008]. There, these gases would undergo conversion to sulfate particles, increasing the planetary albedo and cooling climate,

<sup>1</sup>Institut für Physik der Atmosphäre, Deutsches Zentrum für Luft- und Raumfahrt, Oberpfaffenhofen, Germany.

<sup>2</sup>Institute for Atmospheric Physics, Johannes Gutenberg University, Mainz, Germany.

<sup>3</sup>Atmospheric Physics Division, Max Planck Institute for Nuclear Physics, Heidelberg, Germany.

<sup>4</sup>Particle Chemistry, Max Planck Institute for Chemistry, Mainz, Germany.

which may offset anthropogenic greenhouse warming. However, the effects of such climate engineering are complex [Tilmes *et al.*, 2009] and unforeseen. Adverse effects may occur.

[3] If volcanic chlorine would reach the stratosphere and undergo activation, it would at least temporarily contribute significantly to catalytic destruction of stratospheric ozone. Model studies of Tabazadeh and Turco [1993] attributed efficient scavenging of HCl of at least 99% to HCl dissolution in liquid water droplets, followed by rain out. Later, Textor *et al.* [2003] argued based on model simulations that efficient scavenging of HCl depends on the relative humidity in the eruption column. They found that depending on the type of eruption and the meteorological situation up to 25% of the initially emitted HCl can reach the stratosphere if incorporated into ice particles that form in the eruption column and that are lifted into the stratosphere. Depending on the fate of the ice particles, the HCl might undergo activation and may contribute to stratospheric ozone destruction. In rough agreement with later model simulations, pronounced amounts of HCl have been observed in the lower stratosphere after recent volcanic eruptions. Hunton *et al.* [2005] detected SO<sub>2</sub>, HNO<sub>3</sub>, and HCl in the young eruption plume (35 h) of Mt. Hekla at an altitude of 11.3 km in February 2000. They found elevated HCl levels of up to 80 ppbv above the background where SO<sub>2</sub> was also enhanced. The observed SO<sub>2</sub>/HCl of 14.3 in the UT/LS suggests little scavenging of HCl in the tropospheric eruption column [Rose *et al.*, 2006].

[4] Additionally, NaCl originating from crustal material or from the sea may reach the stratosphere after a major volcanic eruption [Woods *et al.*, 1985]. In the stratosphere, NaCl may react with sulfuric acid (formed from injected SO<sub>2</sub>) leading to the formation of secondary HCl and Na<sub>2</sub>SO<sub>4</sub> in the months after the eruption. Previous spectroscopic measurements made in the stratospheric eruption plume of volcano El Chichón (1982) indicated a local HCl increase of 40% [Mankin and Coffey, 1984]. This increase was attributed to the formation of secondary HCl from NaCl [Woods *et al.*, 1985].

[5] NaCl particles may also react with HNO<sub>3</sub>, NO<sub>2</sub>, ClNO<sub>3</sub>, N<sub>2</sub>O<sub>5</sub> all forming NaNO<sub>3</sub> and either HCl or reactive chlorine species [Michelangeli *et al.*, 1991]. However, in contrast to sulfuric acid, nitric acid does not condense significantly at most stratospheric temperatures (T > 210 K) typical for the latitudes and season of interest.

[6] In summer 2008 several explosive volcanic eruptions took place at high northern latitudes (52 to 53°N) on islands belonging to the Aleutian chain. The eruption plumes reached the stratosphere. Mt. Okmok erupted on 12 July 2008 and injected an estimated amount of 0.2 Mt SO<sub>2</sub> into the atmosphere. Mt. Kasatochi erupted on 7–8 August 2008 and injected about 1.5 Mt SO<sub>2</sub> into the atmosphere as detected by the Ozone Monitoring Instrument (OMI) on NASA's Aura satellite [Carn *et al.*, 2008]. Compared to Okmok, Kasatochi produced a much stronger eruption, with an SO<sub>2</sub> plume altitude of 12.5 ± 4 km [Karagulian *et al.*, 2010]. However, the Kasatochi SO<sub>2</sub> injection was considerably smaller than the SO<sub>2</sub> injections of the previous major explosive eruptions of the tropical volcanoes El Chichón (10 Mt) and Pinatubo (20 Mt; the strongest explosive volcanic SO<sub>2</sub> injection of the 20th century). Nevertheless, Kasatochi is particularly interesting since, in contrast to El Chichón (17.3°N) and Pinatubo (15°N), it represents a high-latitude volcano eruption.

[7] The present paper reports on airborne ITCIMS measurements of SO<sub>2</sub>, HCl, and HNO<sub>3</sub> performed during the CONtrail and Cirrus ExpeRiment (CONCERT) campaign [Voigt *et al.*, 2010] on 31 October 2008 over Europe. Along with ITCIMS measurements, we made measurements of nitrogen oxide NO, NO<sub>y</sub>, O<sub>3</sub>, and CO as well as particulate sulfate in the aged (about 85 days) lower stratospheric plume of volcano Kasatochi. During the CONCERT campaign, for the first time, SF<sub>5</sub><sup>-</sup> reagent ions have been used in combination with the airborne ITCIMS. Therefore we give here a detailed description of the SF<sub>5</sub><sup>-</sup> reaction scheme used for the present employment of the ITCIMS method. In section 3 we show trace gas distributions in the volcanic plume intercepted in the lowest stratosphere. Further we discuss the chemical processing of the trace gases and their impact on ozone.

[8] A companion paper by Schmale *et al.* [2010] concentrates on simultaneous aerosol measurements made with an Aerosol Mass Spectrometer (AMS) on the same research aircraft FALCON during CONCERT.

## 2. Instrumentation

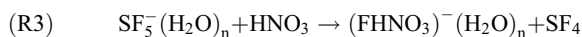
### 2.1. ITCIMS Method

[9] Our measurements in the stratospheric plume of Kasatochi took place on 31 October 2008 aboard the German research aircraft Falcon during two flights, one flight from Munich (Germany) to Shannon (Ireland) and the return flight from Shannon to Munich. The trace gases SO<sub>2</sub>, HCl, and HNO<sub>3</sub> were measured by an ITCIMS instrument, which is a CIMS instrument equipped with an ion trap mass spectrometer.

[10] The ion trap mass spectrometer was configured and extensively employed for atmospheric airborne measurements by MPIK and an MPI-K/DLR collaboration. It has previously been used in combination with O<sub>3</sub><sup>-</sup>, NO<sub>3</sub><sup>-</sup>, CO<sub>3</sub><sup>-</sup>, and NO<sub>3</sub>HNO<sub>3</sub><sup>-</sup> reagent ions for the detection of SO<sub>2</sub>, HNO<sub>3</sub>, HF, HCN, and gas phase sulfuric acid as well as chemion measurements [Kiadler *et al.*, 2000a, 2000b; Fiedler *et al.*, 2005; Speidel *et al.*, 2007; Fiedler *et al.*, 2009a, 2009b, 2010].

[11] For the present measurements, the ion trap mass spectrometer was equipped for the first time with an ion source generating SF<sub>5</sub><sup>-</sup> reagent ions. This reagent ion has been used previously [e.g., Marcy *et al.*, 2004, 2005; Popp *et al.*, 2007] in aircraft-borne CIMS instruments equipped with linear quadrupole mass spectrometers. In addition to the reactions of HCl and HNO<sub>3</sub> with SF<sub>5</sub><sup>-</sup> reported previously, we focus here also on the reaction with SO<sub>2</sub>.

[12] In our ITCIMS instrument (Figure 1) the reagent ions were generated in a radioactive (<sup>210</sup>Po; 20mCi) ion source through which a flow of 2 SLPM carrier gas (N<sub>2</sub> with 1% propane) and 4 SCCM of 600 ppmv SCF<sub>8</sub> in N<sub>2</sub> was passed. In the flow reactor (FR), the reagent ions undergo hydration leading to SF<sub>5</sub><sup>-</sup>(H<sub>2</sub>O)<sub>n</sub> cluster ions, which serve as effective reagent ions. These react with the trace gases SO<sub>2</sub>, HCl, and HNO<sub>3</sub> via the following reactions:



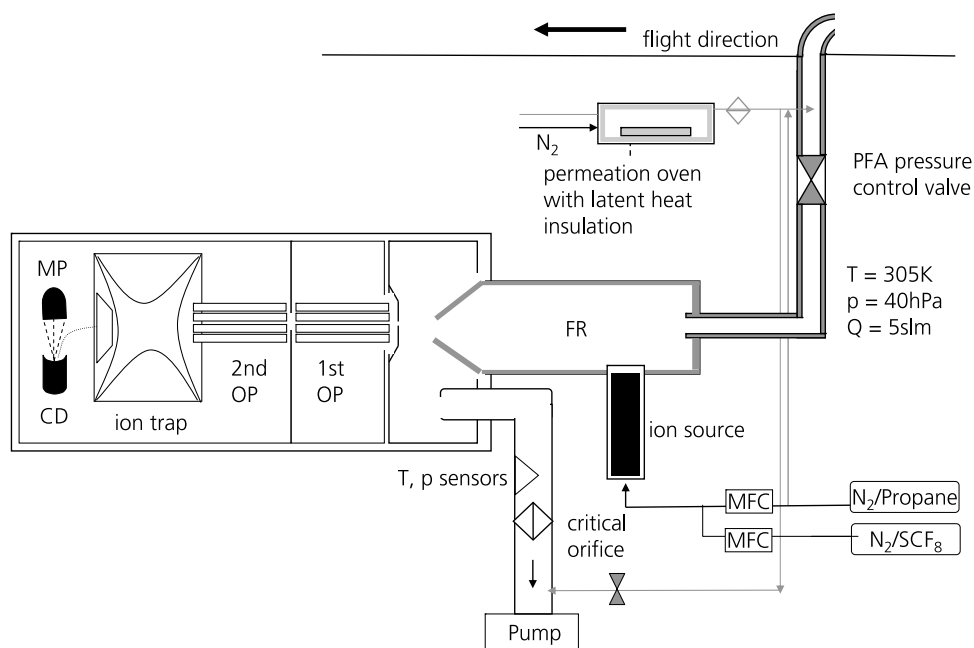


**Figure 1.** Schematic diagram of the ITCIMS instrument. Ion-molecule reactions occur in a flow reactor (FR) with a 40 mm diameter. The ions enter the mass spectrometer through a critical orifice and are guided into the ion trap by two octupoles (OP). After trapping the ions are accelerated toward the conversion dynode (CD) where secondary electrons are produced which are detected by the electron multiplier (MP). For a detailed description, see text.

The mass to charge ratio ( $m/z$ ) of the major dehydrated product ions are 83 ( $\text{FSO}_2^-$ ), 55 and 57 ( $\text{FH}^{35}\text{Cl}^-$  and  $\text{FH}^{37}\text{Cl}^-$ ), and 82 ( $\text{FHNO}_3^-$ ). The ions are guided into the ion trap through a set of octupole (OP) and interoctupole lenses. Upon injection into the ion trap ions undergo dehydration and deceleration due to collisions with helium atoms. A fraction of the dehydrated ions may even undergo additional dissociation. Fragmentation of  $\text{FHCl}^-$  leads to  $\text{Cl}^-$  (35 and 37) and HF; fragmentation of  $\text{FHNO}_3^-$  leads to  $\text{NO}_3^-$  (62) and HF. Fragmentation of  $\text{FSO}_2^-$  may lead to  $\text{F}^-$  (19) but has not been observed. Separation of the two neighboring masses 82 and 83 requires a mass analyzer with a sufficiently high mass resolution, which was for the ion trap optimized to 0.3 atomic mass units (amu) (FWHM). Unequivocal identification of the chemical nature of product ions requires fragmentation of mass selected ions, at least in laboratory tests of the ion reaction scheme. Both requirements are met by the ion trap mass spectrometer used for our measurements. All masses are monitored quasi-simultaneously; during a trapping time of approximately 200 ms, ions with 15 to 170  $m/z$  are sampled. The automatic gain control was applied to achieve a constant ion concentration in the ion trap. The read out time after each trapping comprised approximately 100 ms. Five so-called microscans are averaged to obtain one spectrum with an overall time resolution of 1.6 s. Tuning of the ion trap was performed before the campaign and remained the same for all flights for a better comparison. The tuning procedure scans through the octupole voltages, front plate, and interoctupole lens voltages as well as the multipole radio frequency to obtain the best ion signal for a specific mass. For this

campaign the tuning was optimized for the mass 55 ( $\text{FHCl}^-$ ) resulting in a decreased trapping efficiency for higher masses such as the  $\text{SF}_5^-$  reagent ion.

[13] The CIMS instrument had a specifically designed permeation oven for in-flight  $\text{HNO}_3$ -calibration deployed during the mission. It contained a nitric acid permeation standard in a glass container which was heated to 325 K and maintained at a constant pressure of 2.4 bar. The glass container was embedded in a latent heat reservoir which maintained the temperature for 45 min in case of power shortage. A calibration flow of 110 SCCM was injected through a critical orifice made of glass into the 5 SLPM sample flow at the upper part of the sampling line in front of a PFA pressure control valve. The sampling line was entirely fabricated of or covered with PFA and except for the distance from the aircraft wall to the inlet entrance kept at a pressure of 40 hPa and above a temperature of 305 K to minimize loss of nitric acid to the walls [Neuman *et al.*, 1999]. The calibration flow was continuously pumped away and occasionally injected during the flights by closing a valve in front of the pump thus accounting for the sensitivity and wall losses under the given atmospheric conditions.

[14]  $\text{SO}_2$  and HCl were calibrated after the flights.  $\text{SO}_2$  calibration was performed with a bottled standard in dry nitrogen. HCl calibration was done with a permeation standard and a quantitative analysis was performed with an ion chromatograph, both standards offering 10% accuracy. A cross sensitivity for water vapor mole fractions below 200 ppmv causing an enhanced background signal on mass 83 ( $\text{FSO}_2^-$ ) and mass 55 ( $\text{FHCl}^-$ ) was not observed. Water

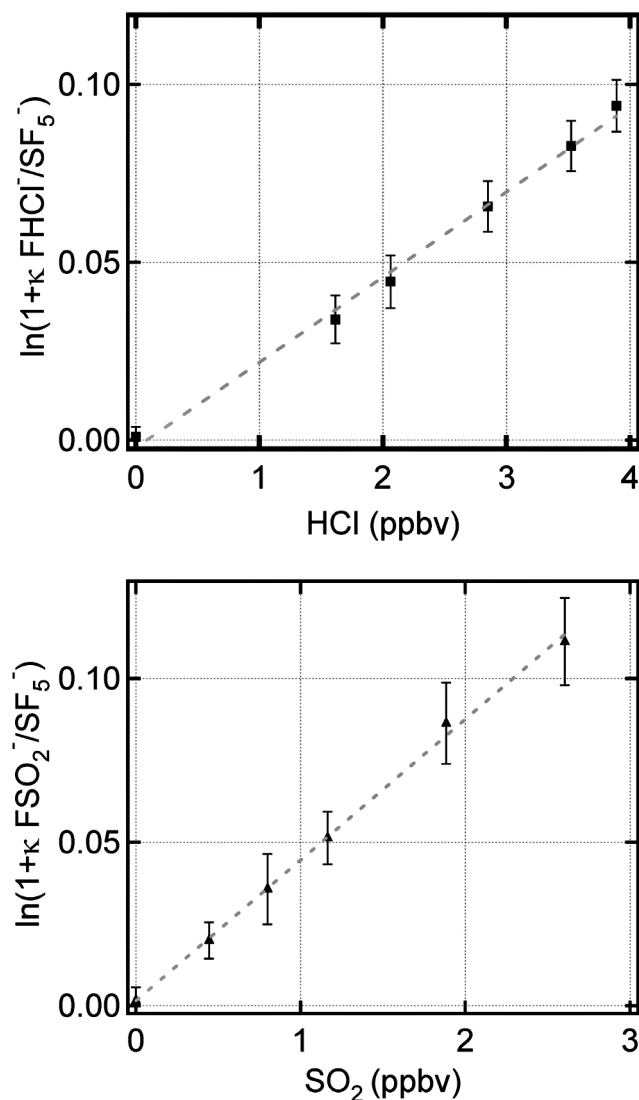


**Figure 2.** Calibration of  $\text{SO}_2$  and HCl in the laboratory. The  $\ln(1 + \kappa R)$  where  $R$  is the ratio of primary product to educt ion and  $\kappa$  the relative mass ion trapping efficiency plotted as a function of  $\text{SO}_2$  and HCl added to the sample flow.

clusters that cause a decrease in the primary ion signal cannot be observed in the ion trap. Ozone interferences for ozone mole fractions smaller than 500 ppbv were tested and had no influence on the measurement.

[15] The calibration factor (CF) was derived under the assumption of a quasi-first-order kinetic reaction leading to the relationship:

$$[A] = CF * \ln\left(1 + \frac{\kappa P^\pm}{E^\pm}\right)$$

Here,  $[A]$  represents the trace gas mole fraction,  $P$  and  $E$  are the ion signals of the product and educt ions, and  $\kappa$  is the relative mass discrimination of the two ions originating from a mass dependent trapping efficiency of the ion trap. The calibration factor  $CF = T^{-1} k^{-1} t_{\text{IMR}}^{-1}$  contains information on the ion molecule reaction time ( $t_{\text{IMR}}$ ) which is usually around

100 ms, the rate coefficient  $k$ , the dilution and the transmission of the sampling line  $T$ . While the  $t_{\text{IMR}}$  and  $k$  are kept constant at low water vapor content, wall effects may vary significantly therefore calibration needs to be done regularly. The calibration factors for HCl were  $42 \pm 6$  ppbv and for  $\text{SO}_2$   $24 \pm 5$  ppbv.

[16] Figure 2 shows laboratory calibrations of HCl and  $\text{SO}_2$ . Here, either HCl or  $\text{SO}_2$  were introduced exclusively. Plotted is  $\ln(\kappa R + 1)$  where  $R$  is the abundance ratio of the primary product ion ( $\text{FHCl}^-$  or  $\text{FSO}_2^-$ ) and the reagent ion  $\text{SF}_5^-$ .

[17] In the stratosphere, the uncertainty in the measured  $\text{SO}_2$ , HCl, and  $\text{HNO}_3$  mixing ratios are estimated to be 25%, 30%, and 30%, respectively. The detection limits ( $1\sigma$  of the background signal) are 0.018 ppbv ( $\text{SO}_2$ , for a running mean over 10 data points), 0.022 ppbv (HCl, running mean over 20 data points), and 0.036 ppbv ( $\text{HNO}_3$ , running mean over 20 data points). Frequent broader variations which may be attributed to electronic interferences from the aircraft affected the precision of the instrument during flights and caused a higher noise in the time sequences. Therefore we chose a running mean over 30 spectra for the HCl measurements. Our statistical analysis however is not affected since it is always based on a large number of data points and therefore should not change the averaged data.

[18] In the troposphere the measurements of  $\text{SO}_2$ , HCl, and  $\text{HNO}_3$  have larger uncertainties due to larger atmospheric water vapor abundance, which may cause interfering reactions and induce undesired wall effects, e.g., the attachment and detachment of sticky molecules in the sampling line.

## 2.2. Chemiluminescence Technique

[19] Reactive nitrogen species ( $\text{NO}_y = \text{NO}, \text{NO}_2, \text{HONO}, \text{HNO}_3, \text{HO}_2\text{NO}_2, \text{N}_2\text{O}_5, \text{PAN} \dots$ ) were measured aboard the Falcon using an  $\text{NO}_y$  detector, which has originally been developed by *Feigl et al.* [1999] on aircraft. The detection principle builds on the chemiluminescence technique [Fahey et al., 1985]. During CONCERT mainly gas phase  $\text{NO}_y$  and NO were measured through two backward facing inlets of the  $\text{NO}_y$  instrument [Ziereis et al., 2000, 2004]. The  $\text{NO}_y$  channel is equipped with a gold converter, where gas phase  $\text{NO}_y$  is catalytically reduced to NO with CO in a gold tube heated to  $300^\circ\text{C}$ . Thereafter the chemiluminescence reaction of NO with  $\text{O}_3$  in the infrared is detected with two photomultipliers. The instrumental error is 10% and the detection limit for NO and  $\text{NO}_y$  is better than 1 pptv and 5 pptv. Aerosol particles with diameters  $< 1 \mu\text{m}$  containing trace amounts of reactive nitrogen may enter the backward facing inlets of the  $\text{NO}_y$  instrument [Feigl et al., 1999]. However, at warm stratospheric conditions ( $T > 210 \text{ K}$ ) as encountered on 31 October 2008, model simulations [Voigt et al., 2007] indicate that the aerosol contribution of  $\text{HNO}_3$  to the  $\text{NO}_y$  concentration is negligible. This is supported by the mass spectrometric aerosol composition measurement performed on board the Falcon showing that particulate nitrate was detected only in the boundary layer aerosol [Schmale et al., 2010].

## 2.3. Aerosol Mass Spectrometry

[20] Particulate sulfate concentrations were measured with an Aerodyne Compact Time-of-Flight Aerosol Mass Spectrometer (AMS) coupled to a pressure controlled inlet (PCI) system by MPI-C. The specific configuration of this

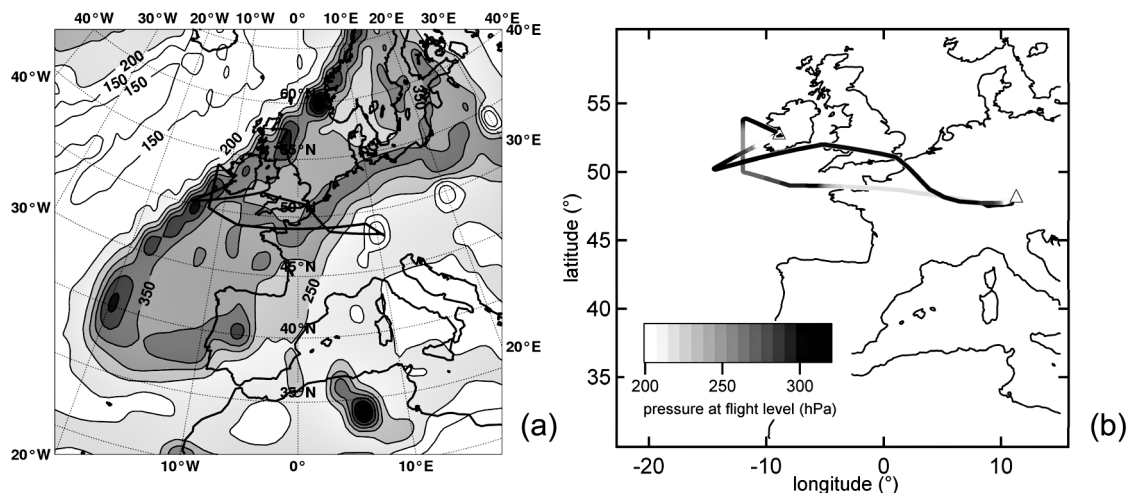


**Figure 3.** (a) Pressure at the tropopause height over Western Europe in hPa along with the flight track of flight A (northern route) and flight B (southern route) and (b) the pressure color coded at flight altitude during the two missions.

AMS instrument, data analysis, and results obtained during CONCERT are described in detail by *Schmale et al.* [2010] and therefore will only be briefly reviewed here. Particulate matter is sampled through a critical orifice in front of an aerodynamic lens system which focuses the particles into a narrow beam. The aerosol is accelerated when entering the time of flight region in the vacuum system. At the end of this chamber the particles are flash-vaporized at approximately 600°C and ionized by electron impact (70 eV) before the ions are extracted into a time-of-flight mass spectrometer. The instrument provides data on chemical composition and size distribution of submicron nonrefractory aerosol particles. For further details, see *Canagaratna et al.* [2007, and references therein]. Particulate sulfate data are reported in  $\mu\text{g m}^{-3}$  (STP). The detection limit for 10 s average data as reported here is 0.05 and 0.03  $\mu\text{g m}^{-3}$  for the two flights on 31 October 2008. The quantifiable precision of the AMS associated with the inlet system is in the order of 30%. Further details on the collection efficiency and the uncertainties of the AMS measurements are discussed by *Schmale et al.* [2010].

### 3. Trace Gas Measurements in the Lowest Stratosphere

#### 3.1. Previous Kasatochi Plume Observations

[21] The objective of the two missions during the CONCERT campaign was to intrude the lower stratosphere, offering an opportunity to intercept the lower stratosphere plume of volcano Kasatochi with the research aircraft Falcon. After the Kasatochi eruption of 7–8 August 2008, the stratospheric eruption plume experienced aging and dilution. Previous to CONCERT satellite borne remote sensing instruments tracked the stratospheric  $\text{SO}_2$  and aerosol plume until early September [*Karagulian et al.*, 2010; *Kristiansen et al.*, 2010]. In addition, *Theys et al.* [2009] reported injection and transport of BrO into the upper troposphere/lower stratosphere region retrieved from GOME 2 satellite observations. Ground-based LIDARs detected the Kasatochi SAP plume in August and September 2008. For example,

ground-based LIDAR data obtained on 3 September 2008 in the Arctic, at Ny Alesund, Svalbard (Spitsbergen) indicate the presence of the plume in the lowermost stratosphere, at altitudes between about 7000 and 11,000 m [*Kristiansen*, 2009]. LIDAR data obtained over Germany revealed the presence of the layer before and after the measurement period [*Schmale et al.*, 2010]. Airborne sampling of particulate sulfate, followed by analysis in the laboratory [*Martinsson et al.*, 2009], indicate that sulfate concentrations were elevated in the lower stratosphere as long as 4 months after the eruption.

#### 3.2. Falcon Missions on 31 October 2008

[22] On 31 October 2008, an extended tongue-shaped region formed over Western Europe with particularly large tropopause pressures (up to 400 hPa, corresponding to tropopause heights as low as about 5000 m). The tongue-shaped feature of a stratospheric streamer indicates that Arctic stratospheric air had intruded to lower latitudes. This was an ideal situation for probing the lower stratosphere by the Falcon as it did allow probing and altitude profiling up to about 6500 m above the tropopause. Figure 3a shows the streamer along with the flight tracks of the aircraft and the corresponding tropopause pressures. The feature built up within three days prior to the measurement and extended from Scandinavia to Portugal. Also shown are the flight tracks of the two missions on 31 October 2008 with the atmospheric pressure at flight level color coded (Figure 3b). Mission A (northern route), with take off at Oberpfaffenhofen, close to Munich (Germany), and landing at Shannon (Ireland), and mission B (return flight, southern route) traversed the tongue-shaped region while cruising in the lower stratosphere, mostly at altitudes between 11,000 and 11,600 m (mission A) and between 9000 and 11,300 m (mission B).

[23] While cruising in the stratospheric air mass, two haze layers were sighted in the lower stratosphere with the bare eye and photographed by the crew aboard the Falcon (Figure 4). The viewing direction of the photograph was approximately northeast. The blue sky above the horizon was hardly visible



**Figure 4.** Photograph of the stratospheric sulfate aerosol layer taken at 1437 UTC, when the Falcon was cruising at 10,000 m altitude. A split layer is clearly visible above the horizon, particularly pronounced in the left part of the photograph.

through the layer, indicating that the layer caused substantial light extinction.

## 4. Results

### 4.1. ITCIMS Mass Spectra

[24] Negative ion mass spectra obtained inside the plume around 9500 m altitude (1457 UTC) and segments of that spectrum are shown in Figure 5. Besides the dehydrated reagent ion  $\text{SF}_5^-$  ( $m/z$  127), two major product ion species  $\text{FHNO}_3^-$  (82) and  $\text{FSO}_2^-$  (83) are present.  $\text{NO}_3^-$  appears partly as a fragment of  $\text{FHNO}_3^-$  and due to contamination from the ion source as demonstrated in our laboratory measurements. Figure 5 (bottom) shows a segment ( $m/z$  54 to 58) of the

same mass spectrum together with a background measurement during the flight. Here the HCl product ions  $\text{FHCl}^-$  ( $m/z$  55 and 57) are clearly elevated above the background. The abundance ratio of the ions 55 and 57 is 2.8, which is within the measurement errors consistent with the terrestrial abundance ratio of the corresponding chlorine atoms ( $^{35}\text{Cl}/^{37}\text{Cl} = 3.13$ ). The discrepancy may be due to an additional ion species with  $m/z$  57.

### 4.2. Time Sequences of $\text{SO}_2$ , HCl, $\text{HNO}_3$ , NO, $\text{NO}_y$ , CO, $\text{O}_3$ , and Aerosol Sulfate

[25] On 31 October 2008 during flight B, the Falcon cruised for an extended period of time (more than 2 h) in the lower stratosphere, as indicated by the dynamical tropopause altitude (gray line) derived from European Centre of Medium Weather Forecast (ECMWF) analysis shown in Figure 6. The vertical cross sections of the temperature (color coded) along the flight path together with the potential temperature ( $\theta$ ) isotherms (black line) mirrors a cut through the tongue-shaped region. In the lower stratosphere, an extended layer with increased  $\text{SO}_2$  was observed (Figure 6a).  $\text{SO}_2$  was almost exclusively enhanced above the background when the aircraft reached altitudes above the 2 PVU (potential vorticity unit) isosurface. Filaments of this stratospheric intrusion reached down to 5000 m above the ground, transporting stratospheric air to low altitudes. Around 1410 UTC the Falcon entered the stratosphere. Here the  $\theta$  isotherms crossed the dynamical tropopause, allowing transport and mixing of tropospheric and stratospheric air. A similar transport occurred at the western side of the fold where the aircraft left the stratosphere and again the isotherms crossed the dynamical tropopause.

[26] The time sequences of  $\text{SO}_2$ , HCl, and  $\text{HNO}_3$  obtained by the ITCIMS instrument aboard the Falcon during the flight A and B are shown in Figure 7. Also given are 10 s averages of the particulate sulfate concentrations, volume mixing ratios of  $\text{O}_3$ , NO,  $\text{NO}_y$ , and CO (all 1 s time resolution) measured aboard the aircraft, the flight altitude, and  $\theta$

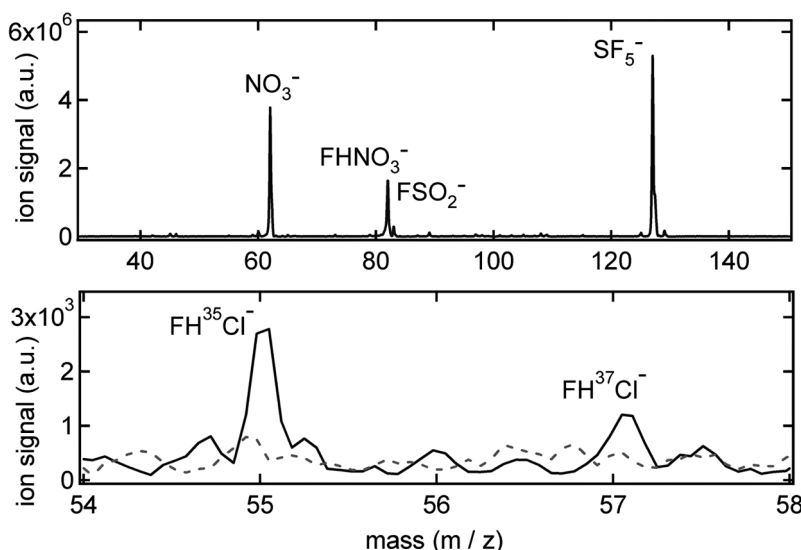


**Figure 5.** (top) A negative ion mass spectrum obtained by the ITCIMS inside the plume around 9500 m altitude (1457 UTC) and (bottom) a segment ( $m/z$  54 to 58) of that spectrum. See text for details.

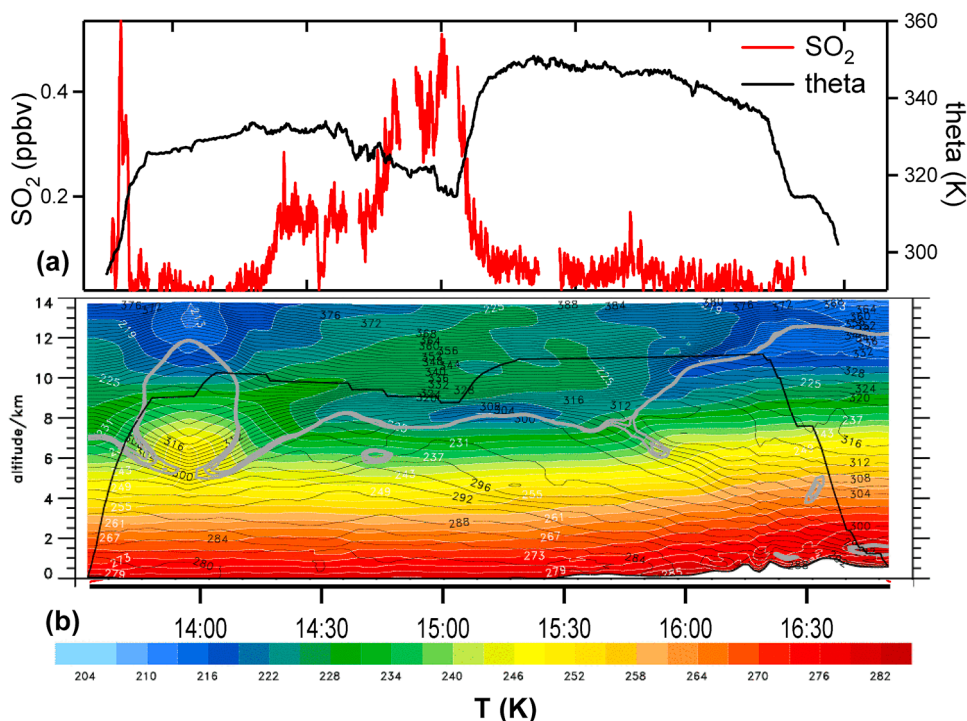


**Figure 6.** (a) Time sequence of  $\text{SO}_2$  mole fractions together with the potential temperature measured onboard the aircraft during flight B. The meteorological data were provided by the European Centre of Medium Weather Forecast (ECMWF). (b) Flight altitude and temperature profile along the flight track (color coded) and potential temperature isotherms (black lines). The gray lines represent the height of the dynamical tropopause (given in 2 potential vorticity units).

along the flight track. Ozone was measured by means of an UV absorption photometer. Using vacuum fluorescence detection, CO was measured at a 1 Hz time resolution.

[27] Gaps in the time sequence appear where calibration or background measurements were performed. The ITCIMS data are smoothed with a running mean over 10 spectra (30 spectra for HCl). The fast and broad variations in the HCl data are due to instrumental counting statistics near the detection limit.

[28] In the following paragraph flight B will be discussed in detail as the plume was most clearly observed during that flight. The aircraft cruised mostly between 9100 and 11,600 m altitude and has spent considerable time (about 1410–1625 UTC) inside a plume with increased  $\text{SO}_2$  mole fractions and enhanced sulfate. The measured  $\text{SO}_2$  reached peak values of up to 0.51 ppbv. Background  $\text{SO}_2$  ranged between 0.02 and 0.055 ppbv. While HCl varied between values below the detection limit (0.044 ppbv,  $2\sigma$ ) to 0.32 ppbv throughout the whole flight, inside the plume HCl ranged from 0.065 ppbv to 0.159 ppbv. CO varied between 38 and 52 ppbv inside the plume with an average of 45 ppbv. Ozone showed peak values of 361 ppbv with an average of 259 ppbv in the stratospheric segment. The time sequences indicate a strong correlation between the measured HCl and  $\text{O}_3$  mole fractions. Nitric oxide was below 0.2 ppbv with the exception of pronounced spikes indicating occasional penetrations of aircraft exhaust plumes.  $\text{NO}_y$  stayed between 1 and 2 ppbv in the stratosphere and is markedly enhanced during

aircraft exhaust plume encounters. Nitric acid showed similar features as  $\text{NO}_y$  except for the aircraft plume penetrations, which is expected as aircraft emit only very little  $\text{HNO}_3$ .

[29]  $\text{SO}_2$  and particulate sulfate reveal similar features during the two flights. In contrast to the broad feature of the  $\text{SO}_2$  and particulate sulfate enhancements in the stratospheric tongue with a horizontal extension of more than 440 km, the Falcon flew through another layer with increased  $\text{SO}_2$  (up to 0.535 ppbv) during the initial ascent from Shannon at 1340 UTC (around 7000 m altitude) which is shown in more detail in Figure 8. Two differently composed air masses both containing increased  $\text{SO}_2$  and particulate sulfate were observed, the lower one between 1340 and 1341 UTC with enhanced CO but  $\text{O}_3$  below 100 ppbv, thus revealing tropospheric character. Between 1341 and 1342 UTC, an  $\text{SO}_2$  layer with decreased CO but increased HCl (up to 0.050 ppbv) and  $\text{O}_3$  up to 125 ppbv was penetrated, showing a stratospheric character. The stratospheric marker HCl implies that this air mass has been mixed downward from higher altitudes transporting ozone into the tropopause region. The upper tropospheric  $\text{SO}_2$  layer may be of volcanic or anthropogenic origin.

#### 4.3. Altitude Profiles of $\text{SO}_2$ , HCl, and $\text{HNO}_3$

[30] Figure 9 shows the altitude profiles of  $\text{SO}_2$ , HCl, and  $\text{HNO}_3$  along with  $\text{O}_3$ , CO mole fractions, and the temperature measured on board the Falcon. The  $\text{SO}_2$  layer was present at altitudes between 7000 and 11,600 m, peaking at 9000 m

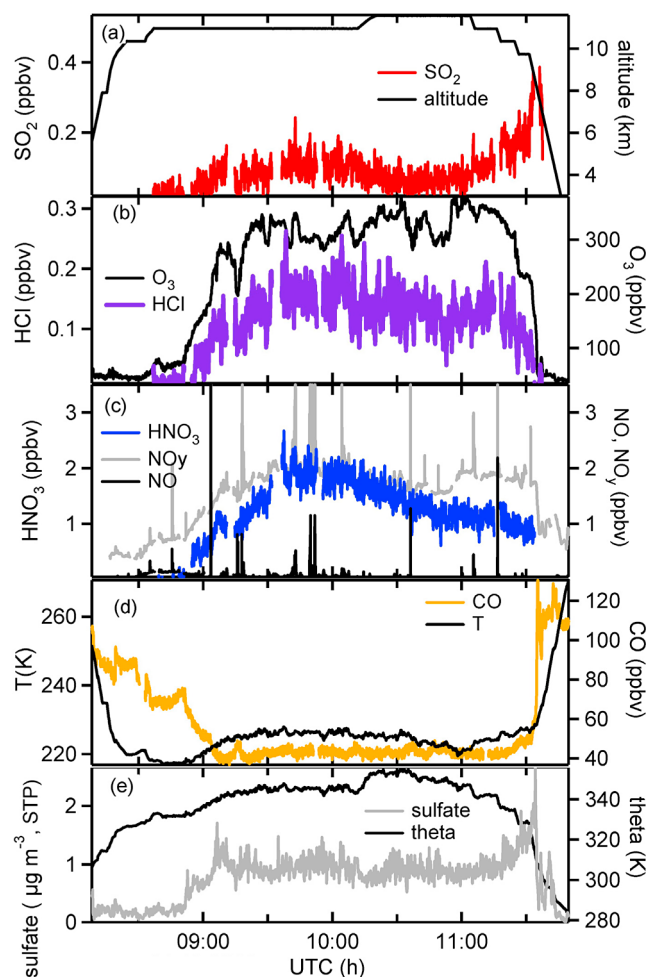


**Figure 7.** Time sequences of  $\text{SO}_2$ , HCl, and  $\text{HNO}_3$  mole fractions obtained by the ITCIMS instrument aboard the Falcon during flights A and B. Also given are particulate sulfate (STP) concentrations,  $\text{O}_3$ , NO,  $\text{NO}_y$ , and CO mole fractions as well as the flight altitude of the aircraft and the potential temperature.

(0.51 ppbv). The second  $\text{SO}_2$ -rich layer was present at lower altitudes extending between about 6400 and 7000 m altitude.

[31] Compared to  $\text{SO}_2$  concentrations in the flight corridors over Germany and Western Europe, measured later during the campaign,  $\text{SO}_2$  showed short-term peaks of similar magnitude (up to 6 ppbv) when intentionally chasing other aircraft and detecting the young aircraft exhaust plume. The  $\text{SO}_2$  background values in the aircraft flight corridors in the troposphere reached 0.09 ppbv at maximum, thus air traffic can be ruled out for this broad  $\text{SO}_2$  layer. Backward trajectories calculated with LAGRANTO [Wernli and Davies, 1997] ending up to 6 days prior to the measurement showed that the air parcels with stratospheric character resided above the tropopause (potential vorticity > 2 PVU). Therefore recent injection of  $\text{SO}_2$  from lower altitudes can also be excluded for the broad stratospheric feature. On the basis of this combined evidence, our working hypothesis is that the stratospheric  $\text{SO}_2$ -rich layer was of volcanic origin, most likely injected by the Kasatochi eruption on 8 August 2008. We cannot exclude additional contribution from other sources nor can a direct

causality be proven, but other sources appear less plausible than our working hypothesis.

## 5. Partitioning of Volcanic Sulfur Species and Transport

[32] The lifetime of  $\text{SO}_2$  in the stratosphere is highly uncertain and depends mainly on OH, which in turn depends on various factors, such as water vapor and ozone abundance, photolysis rates, and transport into the troposphere. We analyze the conversion of  $\text{SO}_2$  to particulate sulfate to derive the e-folding lifetime of  $\text{SO}_2$  in the lowermost stratosphere at high latitudes in autumn.

[33] Taking into account the horizontally inhomogeneous field of the stratospheric streamer, a more illustrative picture of the vertical trace gas distribution of  $\text{SO}_2$  can be drawn with the data plotted against the relative position to the tropopause. To this end, the potential vorticity was derived from ECMWF analysis. Figure 10 shows the altitude profile of  $\text{SO}_2$ , particulate sulfate, and the sulfate mole fractions relative to the total sulfur mole fraction ( $\text{SO}_2 + \text{SO}_4^{2-}$ ) for both flights A and B; the color code represents the ozone mole fraction.

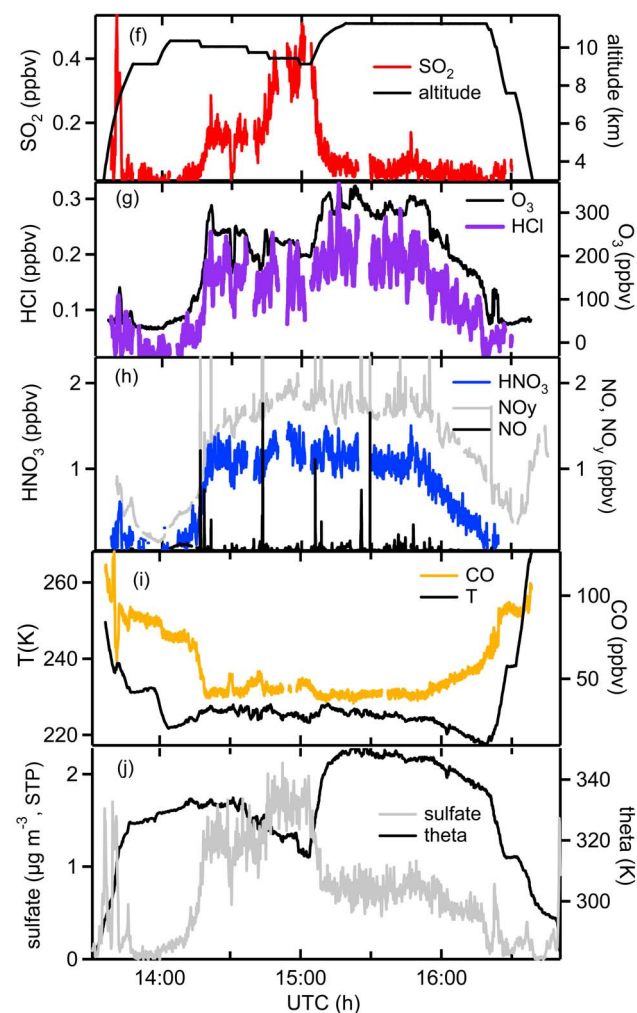


**Figure 7.** (continued)

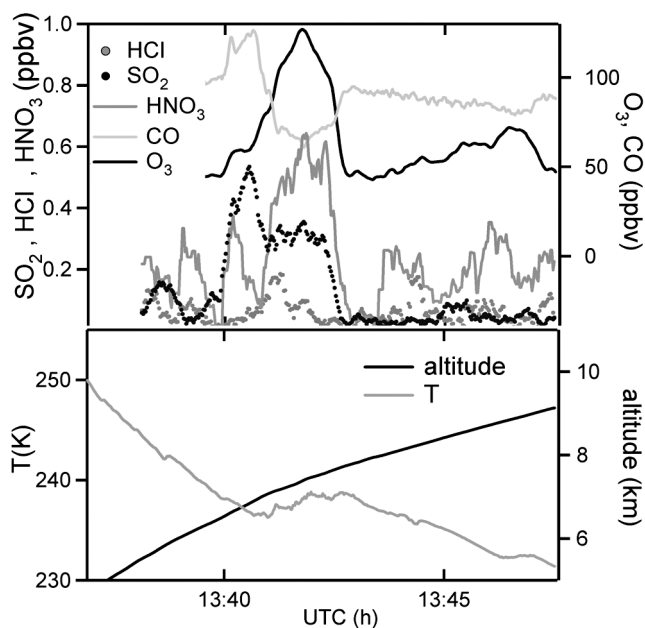


**Figure 8.** Blowup of the segments of Figure 7 which contain the two SO<sub>2</sub>-rich air masses of different origins observed during ascent. (top) HCl, HNO<sub>3</sub>, SO<sub>2</sub>, O<sub>3</sub>, and CO and (bottom) T and the altitude plotted versus time.

Elevated SO<sub>2</sub> and particulate sulfate accompanied by elevated O<sub>3</sub> (>150 ppbv) is found predominantly above the 2 PVU isoline. A second layer of SO<sub>2</sub> and particulate sulfate accompanied by O<sub>3</sub> below 150 ppbv is found below the dynamical tropopause revealing a more tropospheric character. The sulfur rich stratospheric layer was encountered during both flights on 31 October between 1.5 and 2.5 km above the tropopause. We observe similar features and clearly enhanced SO<sub>2</sub> and sulfate mixing ratios in the lower stratosphere.

[34] The ratio  $(\text{SO}_4^{2-}/(\text{SO}_2 + \text{SO}_4^{2-}))$  reflects the fraction of sulfur that has been converted to sulfuric acid and condensed to particulate sulfate. Stratospheric background concentrations have been estimated for both species and subtracted. Maximum stratospheric sulfate background concentrations of  $0.5 \mu\text{g m}^{-3}$  have been measured extensively shortly before the eruption [Schmale *et al.*, 2010]. The SO<sub>2</sub> background mole fraction in the stratosphere has been estimated from our data and adds an uncertainty of about  $\pm 15\%$  to the method. A background value of 0.055 ppbv has been used. The background for both species may partly be caused by injection of sulfur from the Mt. Okmok eruption in July. However, the SO<sub>2</sub> emission from Mt. Okmok was 10 times smaller than the Kasatochi emission and is included in our background correction of SO<sub>2</sub> and the sulfate mole fractions.

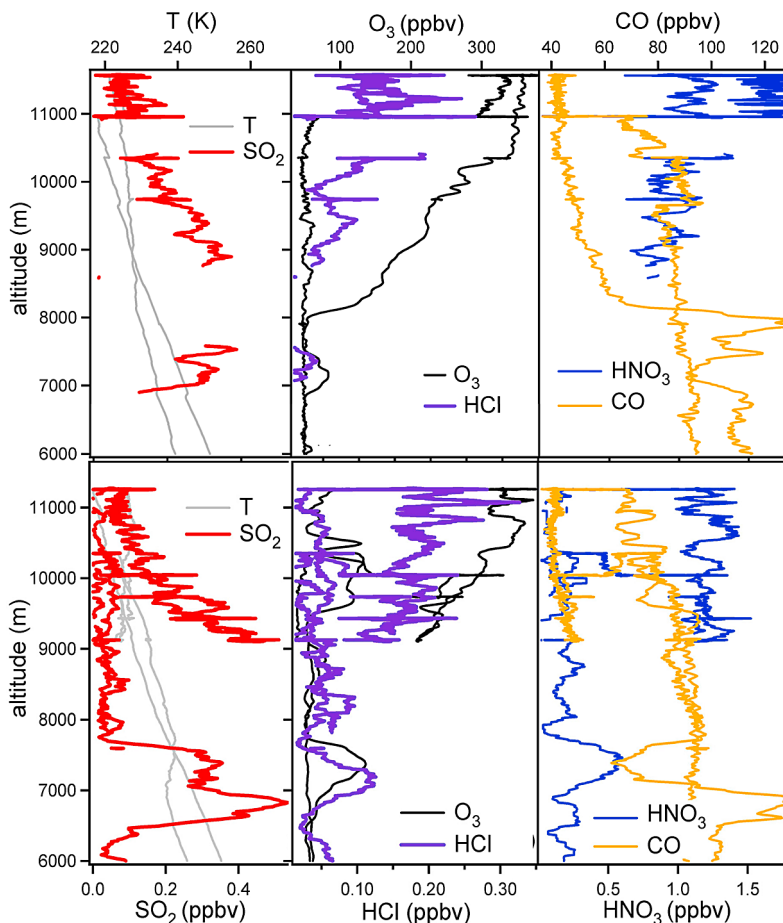


**Figure 9.** Altitude profiles of SO<sub>2</sub>, HCl, and HNO<sub>3</sub> along with O<sub>3</sub>, CO, and the temperature for (top) flight A and (bottom) flight B.

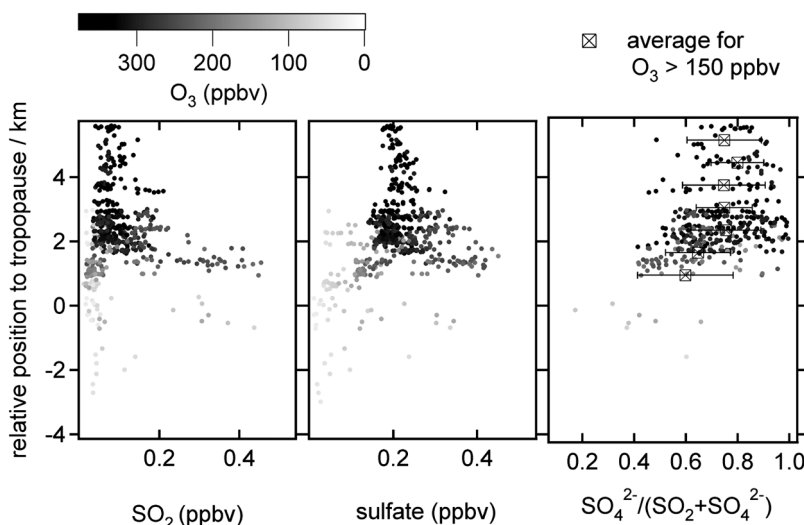


**Figure 10.** Altitude profiles (relative position to the ECMWF model tropopause (2 PVU)) of (left)  $\text{SO}_2$ , (center) particulate sulfate ( $\text{SO}_4^{2-}$ ), and (right) the fraction of converted sulfur ( $\text{SO}_4^{2-}/(\text{SO}_2 + \text{SO}_4^{2-})$ ) with the ozone mole fraction color coded. The data are averaged over 30 s. Bin averages for 0.7 km bins for data points with  $\text{O}_3 > 150$  ppbv have been calculated. The error bars represent the standard deviation of the data points within the bin.

[35] The ratio ( $\text{SO}_4^{2-}/(\text{SO}_2 + \text{SO}_4^{2-})$ ) tends to increase with increasing distance to the tropopause, possibly due to removal of sulfate by cloud processes, particularly ice cloud processes near and below the tropopause. On the other hand, mixing of tropospheric  $\text{SO}_2$  into the layer near the tropopause may have been a reason for the shift in the ratio.

[36] An upper limit of the e-folding lifetime of  $\text{SO}_2$  with respect to OH conversion can be derived for unperturbed air masses at an altitude  $> 1.5$  km above the tropopause. Here 0.7 km-bin averages of the ( $\text{SO}_4^{2-}/(\text{SO}_2 + \text{SO}_4^{2-})$ ) ratios range between 0.73 and 0.82. The ratio inside the densest part of the plume is  $0.75 \pm 0.12$  leading to an e-folding lifetime of 62 days. This value is an upper limit for air masses in the lowermost stratosphere at high latitudes in autumn. The observed conversion ratio compares reasonably well to model simulations by *Kristiansen* [2009] with an e-folding lifetime of 47 days.

## 6. Correlation Analysis

[37] The following discussion is focused on the analysis of the trace gases HCl and  $\text{HNO}_3$  together with  $\text{NO}_y$  inside the stratospheric  $\text{SO}_2$ -rich plume observed during flight B. Both trace gases are abundant in the stratosphere with strong vertical gradients. Variations in their abundance can be compared to regions without volcanic influence when correlated with ozone. Ozone is produced in similar regions in the middle and upper stratosphere as  $\text{HNO}_3$  and HCl therefore downward transport into the lower stratosphere should preserve their relative mixing state if tropospheric sources and chemical or photolytic processes can be neglected [*Marcy et al.*, 2004]. A somewhat conservative criterion of 0.2 ppbv  $\text{SO}_2$  has been set to distinguish the air mass massively influenced by volcanic injection from the less perturbed stratospheric air. Only for measurements in the main plume with high  $\text{SO}_2$  values a significant trend can be expected.

### 6.1. Correlation of HCl With Ozone

[38] A scatterplot of HCl versus  $\text{O}_3$  for flight B with the color code indicating the  $\text{SO}_2$  mole fraction above 0.2 ppbv is shown in Figure 11. Bin averages for ozone bin widths of 30 ppbv have been calculated for air masses inside and outside of the main plume. For air masses with  $\text{SO}_2$  mole fractions smaller than 0.2 ppbv (gray symbols), and for  $\text{O}_3 > 150$  ppbv a linear correlation of  $\text{HCl} = 6.3 \times 10^{-4} \times \text{O}_3 - 0.0036$  is found ( $R^2 = 0.64$ ). This compares well within the measurement uncertainties with previous observations of *Marcy et al.* [2004] with a slope of  $5.2 \times 10^{-4}$  in stratospheric air not influenced by relatively recent major volcanic erup-

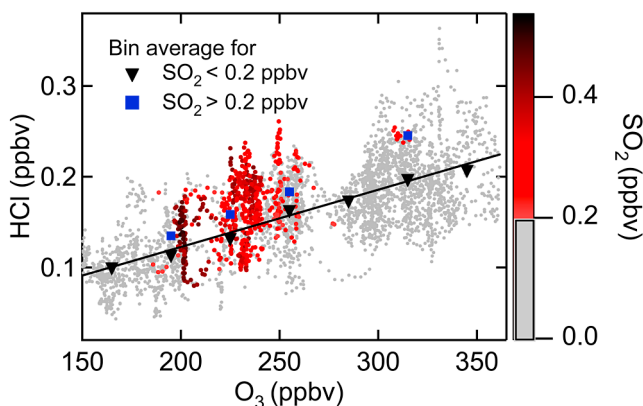


**Figure 11.** Scatterplot of HCl versus  $\text{O}_3$  obtained on 31 October 2008 during mission flight B. The color code indicates the  $\text{SO}_2$  mole fraction for data points where  $\text{SO}_2 > 0.2$  ppbv while the gray dots represent HCl values for  $\text{SO}_2 < 0.2$  ppbv. Bin averages (30 ppbv ozone bins) for  $\text{SO}_2 > 0.2$  ppbv (blue squares) and  $\text{SO}_2 < 0.2$  ppbv (black triangles) have been calculated. The fit (black line) for data points with  $\text{SO}_2 < 0.2$  ppbv has a slope of  $6.3 \times 10^{-4}$ .

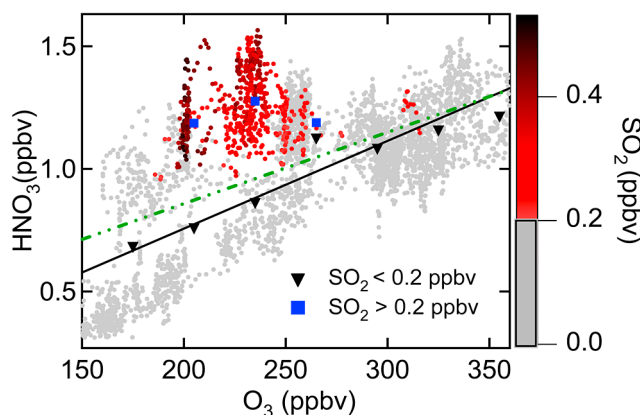


**Figure 12.** Scatterplot of  $\text{HNO}_3$  versus  $\text{O}_3$ . The color code indicates the  $\text{SO}_2$  mole fraction. Two fits are included, one for all data  $\text{O}_3 > 150$  ppbv and one for data points  $\text{O}_3 > 150$  ppbv and  $\text{SO}_2 < 0.2$  ppbv. Bin averages are calculated for inside ( $\text{SO}_2 > 0.2$  ppbv) (blue squares) compared to outside plume conditions ( $\text{SO}_2 < 0.2$  ppbv) (black triangles).

tions at lower latitudes. The larger slope of our data set may be due to a latitude dependence of the ratio [Marcy *et al.*, 2004]. For plume parcels with  $\text{SO}_2$  mole fractions  $> 0.2$  ppbv (blue squares), the observed HCl bin average tends to be increased by 0.025 ppbv. This suggests an enhancement of 19% compared to plume parcels with  $\text{SO}_2$  mole fractions  $< 0.2$  ppbv (black triangles). The errors of the means are not included but they are at maximum 6%. The increase of the HCl mixing ratio of 19% is within the instrumental errors of our measurements with a precision of 20%. However, all HCl bin averages in the plume with  $\text{SO}_2$  mole fractions  $> 0.2$  ppbv lie above their reference values outside of the plume, which supports our hypothesis. We made sensitivity studies on the threshold for the comparison of plume to nonplume conditions. For an  $\text{SO}_2$  threshold of 0.1 ppbv as compared to 0.2 ppbv, the values for the excess HCl (dHCl) are a bit higher with absolute values between 0.026 to 0.033 ppbv and relative values between 21% and 24%. These values would not significantly change the conclusions.

[39] We cannot rule out that the shift in the bin averages may also be caused by an ozone reduction (up to 40 ppbv would be required). Some reduction should result from incomplete mixing of initially  $\text{O}_3$ -poor tropospheric plume air with ambient  $\text{O}_3$ -rich stratospheric air. With increasing plume age, the  $\text{O}_3$ -deficit decreases due to entrainment of ambient  $\text{O}_3$ -rich stratospheric air into the plume. A quantification of this  $\text{O}_3$ -deficit requires detailed quantitative information on plume dilution, which is not available. It is, at least, also conceivable that  $\text{O}_3$  destruction may have occurred in the lower stratosphere. The excess HCl mole fraction of 0.025 ppbv in the Kasatochi main plume represents at least an upper limit and will be our working hypothesis for the following consideration.

[40] An HCl increase may have occurred through direct injection of volcanic HCl into the stratosphere. Alternatively, it may reflect formation of secondary HCl in the stratosphere induced by sulfuric acid through conversion of injected NaCl. Little is known about the amount of NaCl particles injected into the stratosphere. Secondary HCl formation may take weeks and therefore secondary HCl may not be present

in substantial amounts in the first days after the eruption but only after several months. An upper limit of particulate chloride in the aged plume can be derived from the AMS data [Schmale *et al.*, 2010]. The 30 s detection limit of  $0.03 \mu\text{g m}^{-3}$  (STP) for particulate chloride corresponds to a mixing ratio of 0.019 ppbv. Temperatures in August to October may not have been low enough to allow for the dissolution of HCl in the already very acidic sulfate particles. For heterogeneous chlorine activation by reactions involving HCl, temperatures below 200 K are required [Keim *et al.*, 1996; Borrmann *et al.*, 1997]. Such low temperatures are usually not met in the midlatitude lower stratosphere between August and October; thus heterogeneous activation with respect to chlorine is unlikely to have played a significant role. In the following consideration we therefore neglect ozone depletion caused by heterogeneous activation of HCl on SAP.

[41] The emission ratio of volcanoes for HCl is variable and different for explosive eruptions [Edmonds *et al.*, 2001] still volcanoes are thought not to contribute significantly to the stratospheric chlorine budget [Solomon, 1999]. Hunton *et al.* [2005] detected a ratio  $\text{SO}_2/\text{HCl}$  of 14.3 in the lower stratosphere 35 h after an eruption event of Mt Hekla in 2000, suggesting that no significant scavenging of HCl occurred [Rose *et al.*, 2006]. Satellite measurements made by Microwave Limb Sounder (MLS) [Froidevaux *et al.*, 2008] and OMI indicate an  $\text{SO}_2/\text{HCl}$  molar ratio of 70 after the eruption of Kasatochi, at atmospheric pressure levels of 147 hPa (S. Carn, personal communication, 2009). This ratio has been observed 3 days after the main eruptions, when tropospheric removal processes and loss of gaseous HCl have ceased and is larger than the ratio ( $\sim 50$ ) observed after the Okmok eruption. The molar ratio of total excess sulfur to excess HCl has been calculated from our data. A ratio between 19 and 26 has been found for the lower stratosphere. This ratio is lower (by a factor of 2 to 3) than satellite observations of HCl and  $\text{SO}_2$  in the young eruption plume. The difference may arise from the fact that one layer in the lower stratosphere is compared to a ratio measured at one pressure level. It may also be attributed to secondary HCl formation from injected NaCl, a process of unknown efficiency. Additionally removal of either species due to condensation on and coagulation of sulfate aerosol with ash particles during the first days may have caused a shift in the ratio. However, the satellite measurements as well as our in situ measurements give indications that significant amounts of HCl from Mt. Kasatochi have reached the stratosphere.

## 6.2. Correlation of $\text{HNO}_3$ and $\text{NO}_y$ With Ozone

[42] Figure 12 shows a scatterplot of  $\text{HNO}_3$  versus  $\text{O}_3$ . The color code indicates the  $\text{SO}_2$  mole fraction. The correlation analysis has been limited to a pure stratospheric branch ( $\text{O}_3 > 150$  ppbv) and outside plume conditions ( $\text{SO}_2 < 0.2$  ppbv) with a fit  $\text{HNO}_3 = 3.6 \times 10^{-3} \times \text{O}_3 + 0.04$  (all given in ppbv) (black line). The comparison of the  $\text{HNO}_3/\text{O}_3$  ratio to previous measurements in the lower stratosphere is complicated by the fact that latitudes of interest ( $47^\circ$  to  $54^\circ\text{N}$ ) are not covered by polar data from Schneider *et al.* [1999] and data for latitudes  $> 68^\circ\text{N}$  and  $< 43^\circ\text{N}$  from Popp *et al.* [2009]. Given an increasing slope of the  $\text{HNO}_3/\text{O}_3$  ratio with increasing latitude, our measurements correspond well to previous results [Popp *et al.*, 2009] and extend the detection region for northern mid latitudes. However, this slope

is shifted toward a lower value ( $\sim 2.9 \times 10^{-3}$ , green line) if all data points are fitted, thus illustrating again a profound volcanic influence on the stratospheric inheritance of the  $\text{HNO}_3/\text{O}_3$  relationship. The molar abundance ratios of  $\text{HNO}_3/\text{NO}_y$  have been calculated ranging from 0.51 to 0.72. They compare well with the ratios previously measured [Schneider et al., 1999; Neuman et al., 2001]. Comparison of air masses with  $\text{SO}_2 > 0.2$  ppbv with a ratio of 0.68 and  $\text{SO}_2 < 0.2$  ppbv with a ratio of 0.57, an increase of the  $\text{HNO}_3/\text{NO}_y$  ratio of 19% has been observed. For stratospheric air masses ( $\text{O}_3 > 150$  ppbv) the bin-averaged  $\text{HNO}_3$  (Figure 12) have been calculated, divided into air masses inside ( $\text{SO}_2 > 0.2$  ppbv, blue squares) and outside of the plume ( $\text{SO}_2 < 0.2$  ppbv, black triangles).  $\text{HNO}_3$  is elevated by up to 50% for inside plume conditions compared to the background. The increase of the  $\text{HNO}_3/\text{NO}_y$  ratio is within the instrumental errors while the increase of up to 50% in the  $\text{HNO}_3$  mixing ratios is statistically significant.

[43] Transport of air masses from higher latitudes might partially explain the  $\text{HNO}_3$  increase. Initial injection of  $\text{HNO}_3$  by the volcano or lightning induced  $\text{NO}_x$  as discussed by Rose et al. [2006] cannot explain the observed increase in the  $\text{HNO}_3/\text{O}_3$  ratio. A measured  $\text{dSO}_2/\text{dHNO}_3$  molar ratio of 0.7 for the present measurements would correspond to an initial  $\text{dSO}_2/\text{dHNO}_3$  ratio of 3.5, considering that 80% of the  $\text{SO}_2$  was converted since the eruption. This is an order of magnitude lower than former measurements with yielded ratios between 15 and 250 [Mather et al., 2004b; Rose et al., 2006]. In addition, an increase of  $\text{HNO}_3$  and the  $\text{HNO}_3/\text{NO}_y$  ratio could result from the increased efficiency of  $\text{NO}_x$  conversion to  $\text{HNO}_3$  in the aerosol-rich volcanic plume. There are two stratospheric  $\text{HNO}_3$  formation processes: (1) reaction of  $\text{NO}_2$  with OH; (2) formation of  $\text{N}_2\text{O}_5$  followed by  $\text{N}_2\text{O}_5$  hydrolysis on  $\text{H}_2\text{SO}_4\text{-H}_2\text{O}$  aerosols or PSCs. In most conditions process 2 is not very efficient in the stratosphere. However, in a volcanic plume or in polar air masses containing PSCs the efficiency of process 2 may be significantly increased, due to an increased surface area density of  $\text{H}_2\text{O}$  containing aerosols. Process 2 almost saturates when most  $\text{N}_2\text{O}_5$  formed undergoes hydrolysis rather than photolysis or reaction with OH [Arnold et al., 1990]. This is expected for an  $\text{H}_2\text{SO}_4\text{-H}_2\text{O}$  surface area density larger than about  $10 \mu\text{m}^2 \text{cm}^{-3}$  [Fahey et al., 1993].

## 7. Summary and Conclusions

[44] An airborne ITCIMS instrument has, for the first time, been combined with  $\text{SF}_5^-$  reagent ions and the combination has been deployed on aircraft. The measurements took place on the research aircraft Falcon during the CONCERT campaign in October 2008, where the ITCIMS measured gaseous  $\text{SO}_2$ , HCl, and  $\text{HNO}_3$ . Other instruments on the Falcon detected NO,  $\text{NO}_y$ ,  $\text{O}_3$ , CO, and particulate sulfate. Our airborne trace gas and particle measurements allow for the classification of different air parcel mixing states in the tropopause region using tropospheric and stratospheric tracers. They represent an important contribution for a fundamental understanding of trace gas distributions in the lower stratosphere where only few measurements are available.

[45] On 28 and 31 October 2008, a layer with strongly increased  $\text{SO}_2$  ( $\sim$ factor of 10) and substantially increased HCl (19%) was detected over Europe in the lowermost

stratosphere at altitudes between 7000 and 11,600 m most likely originating from the eruption of the Aleutian volcano Kasatochi. For the molar ratio  $\text{HNO}_3/\text{NO}_y$  an upper limit increase of 19% was obtained from our data. Large SAP surface areas as observed after the volcanic eruption can enhance  $\text{NO}_x$  conversion to  $\text{HNO}_3$  via  $\text{N}_2\text{O}_5$  hydrolysis.

[46] Excess  $\text{SO}_2$  ( $\text{dSO}_2$ ) reached about 0.45 ppbv and excess HCl ( $\text{dHCl}$ ) reached about 0.025 ppbv in the volcanic plume, implying that  $\text{SO}_2$  and HCl have been injected into the stratosphere by the volcano. The e-folding lifetime of  $\text{SO}_2$  in the lowermost stratosphere at high latitudes in autumn was derived from the fraction of particulate sulfate to total sulfur ( $\text{SO}_4^{2-}/(\text{SO}_2 + \text{SO}_4^{2-})$ ). An average value of  $0.75 \pm 0.12$  has been observed in the densest part of the plume. This implies an upper limit of the e-folding  $\text{SO}_2$ -lifetime of about 62 days. As the OH concentrations in the volcanic plume at the northern latitude tropopause are only poorly constrained, our measurements represent a new independent approach to estimate the  $\text{SO}_2$  lifetime in the lower stratosphere.

[47] **Acknowledgments.** This work was partially financed by the junior research group AEROTROP (<http://www.pa.op.dlr.de/AEROTROP>). Part of this work was performed within the DFG SPP 1294 HALO. One of the authors (Frank Arnold) was also funded by the Max Planck Society via the "Max Planck award for Physics"; the Falcon aircraft operation was funded by DLR within the CATS project (<http://www.pa.op.dlr.de/CATS>). The authors would like to thank the flight department for their excellent cooperation during the CONCERT campaign. We acknowledge Dennis Stich who performed trajectory calculations with LAGRANTO. We especially thank David Fahey and Troy Thornberry for helpful discussions.

## References

- Arnold, F., and T. Bührke (1983), New  $\text{H}_2\text{SO}_4$  and  $\text{HSO}_3$  vapour measurements in the stratosphere - Evidence for a volcanic influence, *Nature*, **301**, 293–295, doi:10.1038/301293a0.
- Arnold, F., T. Bührke, and S. Qiu (1990), Evidence for stratospheric ozone-depleting heterogeneous chemistry on volcanic aerosols from El Chichón, *Nature*, **348**, 49–50, doi:10.1038/348049a0.
- Arnold, F., J. Curtius, S. Spreng, and T. Deshler (1998), Stratospheric aerosol-sulfuric acid: First direct in-situ measurements using a novel balloon-based mass spectrometer apparatus, *J. Atmos. Chem.*, **30**, 3–10, doi:10.1023/A:1006067511568.
- Borrmann, S., et al. (1997), Heterogeneous reactions on stratospheric background aerosols, volcanic sulfuric acid droplets, and type I polar stratospheric clouds: Effects of temperature fluctuations and differences in particle phase, *J. Geophys. Res.*, **102**(D3), 3639–3648, doi:10.1029/96JD02976.
- Caldeira, K., and L. Wood (2008), Global and Arctic climate engineering: Numerical model studies, *Phil. Trans. R. Soc. London, Ser. A*, **366**, 4039–4056, doi:10.1098/rsta.2008.0132.
- Canagaratna, M. R., et al. (2007), Chemical and microphysical characterization of ambient aerosols with the aerodyne aerosol mass spectrometer, *Mass Spectrom. Rev.*, **26**(2), 185–222, doi:10.1002/mas.20115.
- Cam, S. A., N. A. Krotkov, V. Fioletov, K. Yang, A. J. Krueger, and D. Tarasick (2008), Emission, transport and validation of sulfur dioxide in the 2008 Okmok and Kasatochi eruption clouds, *Eos Trans. AGU*, **89**(53), Fall Meet. Suppl., Abstract A51J–07.
- Crutzen, P. (2006), Albedo enhancement by stratospheric sulfur injections: A contribution to resolve a policy dilemma?, *Clim. Change*, **77**(3–4), 211–220, doi:10.1007/s10584-006-9101-y.
- Dutton, E. G., and J. Christy (1992), Solar radiative forcing at selected locations and evidence for global lower tropospheric cooling following the eruptions of El Chichón and Pinatubo, *Geophys. Res. Lett.*, **19**(23), 2313–2316, doi:10.1029/92GL02495.
- Edmonds, M., D. Pyle, and C. Oppenheimer (2001), A model for degassing at the Soufrière Hills Volcano, Montserrat, West Indies, based on geochemical data, *Earth Planet. Sci. Lett.*, **186**(2), 159–173, doi:10.1016/S0012-821X(01)00242-4.
- Fahey, D. W., C. S. Eubank, G. Hubler, and F. C. Fehsenfeld (1985), Evaluation of a catalytic reduction technique for the measurement of total

- reactive odd-nitrogen  $\text{NO}_x$  in the atmosphere, *J. Atmos. Chem.*, **3**, 435–468, doi:10.1007/BF00053871.
- Fahey, D. W., et al. (1993), In situ measurements constraining the role of sulfate aerosols in mid-latitude ozone depletion, *Nature*, **363**(6429), 509–514, doi:10.1038/363509a0.
- Feigl, C., H. Schlager, H. Ziereis, J. Curtius, F. Arnold, and C. Schiller (1999), Observation of  $\text{NO}_x$  uptake by particles in the Arctic tropopause region at low temperatures, *Geophys. Res. Lett.*, **26**(14), 2215–2218, doi:10.1029/1999GL900338.
- Fiedler, V., et al. (2005), The contribution of sulphuric acid to atmospheric particle formation and growth: A comparison between boundary layers in Northern and Central Europe, *Atmos. Chem. Phys.*, **5**, 1773–1785, doi:10.5194/acp-5-1773-2005.
- Fiedler, V., R. Nau, S. Ludmann, F. Arnold, H. Schlager, and A. Stohl (2009a), East Asian  $\text{SO}_2$  pollution plume over Europe—Part 1: Airborne trace gas measurements and source identification by particle dispersion model simulations, *Atmos. Chem. Phys.*, **9**, 4717–4728, doi:10.5194/acp-9-4717-2009.
- Fiedler, V., F. Arnold, H. Schlager, A. Dörnbrack, L. Pirjola, and A. Stohl (2009b), East Asian  $\text{SO}_2$  pollution plume over Europe—Part 2: Evolution and potential impact, *Atmos. Chem. Phys.*, **9**, 4729–4745, doi:10.5194/acp-9-4729-2009.
- Fiedler, V., F. Arnold, S. Ludmann, A. Minikin, L. Pirjola, A. Dörnbrack, and H. Schlager (2010), African biomass burning plumes over the Atlantic: Aircraft based measurements and implications for  $\text{H}_2\text{SO}_4$  and  $\text{HNO}_3$  mediated smoke particle activation, *Atmos. Chem. Phys. Discuss.*, **10**, 7699–7743, doi:10.5194/acpd-10-7699-2010.
- Froidevaux, L., et al. (2008), Validation of Aura Microwave Limb Sounder HCl measurements, *J. Geophys. Res.*, **113**, D15S25, doi:10.1029/2007JD009025.
- Hanson, D., and A. Ravishankara (1991), The reaction probabilities of  $\text{ClONO}_2$  and  $\text{N}_2\text{O}_5$  on 40 to 75% sulfuric acid solutions, *J. Geophys. Res.*, **96**(D9), 17,307–17,314, doi:10.1029/91JD01750.
- Hunton, D., et al. (2005), In-situ aircraft observations of the 2000 Mt. Hekla volcanic cloud: Composition and chemical evolution in the Arctic lower stratosphere, *J. Volcanol. Geotherm. Res.*, **145**(1–2), 23–34, doi:10.1016/j.jvolgeores.2005.01.005.
- Karagulian, F., L. Clarisse, C. Clerbaux, A. J. Prata, D. Hurtmans, and P. F. Coheur (2010), Detection of volcanic  $\text{SO}_2$ , ash and  $\text{H}_2\text{SO}_4$  using the IASI sounder, *J. Geophys. Res.*, **115**, D00L02, doi:10.1029/2009JD012786.
- Keim, E. R., et al. (1996), Observations of large reductions in the  $\text{NO}/\text{NO}_y$  ratio near the mid-latitude tropopause and the role of heterogeneous chemistry, *Geophys. Res. Lett.*, **23**(22), 3223–3226, doi:10.1029/96GL02593.
- Kiendler, A., S. Aberle, and F. Arnold (2000a), Negative chemions formed in jet fuel combustion: New insights from jet engine and laboratory measurements using a quadrupole ion trap mass spectrometer apparatus, *Atmos. Environ.*, **34**, 2623–2632, doi:10.1016/S1352-2310(99)00475-6.
- Kiendler, A., S. Aberle, and F. Arnold (2000b), Positive ion chemistry in the exhaust plumes of an aircraft jet engine and a burner: Investigations with a quadrupole ion trap mass spectrometer, *Atmos. Environ.*, **34**, 4787–4793, doi:10.1016/S1352-2310(00)00253-3.
- Kristiansen, N. I. (2009), Determination of the emission height profile of volcanic emissions using inverse modelling, M. S. thesis, Univ. of Oslo, Oslo, Norway.
- Kristiansen, N. I., et al. (2010), Remote sensing and inverse transport modeling of the Kasatochi eruption sulfur dioxide cloud, *J. Geophys. Res.*, doi:10.1029/2009JD013286, in press.
- Mankin, W. G., and M. T. Coffey (1984), Increased stratospheric hydrogen chloride in the El Chichón cloud, *Science*, **226**(4671), 170–172, doi:10.1126/science.226.4671.170.
- Marcy, T. P., et al. (2004), Quantifying stratospheric ozone in the upper troposphere with in situ measurements of HCl, *Science*, **304**(5668), 261–265, doi:10.1126/science.1093418.
- Marcy, T. P., R. S. Gao, M. J. Northway, H. Stark, and D. W. Fahey (2005), Using chemical ionization mass spectrometry for detection of  $\text{HNO}_3$ , HCl and  $\text{ClONO}_2$  in the atmosphere, *Int. J. Mass Spectrom.*, **243**, 63–70, doi:10.1016/j.jms.2004.11.012.
- Martinsson, B. G., et al. (2009), Influence of the 2008 Kasatochi volcanic eruption on sulfurous and carbonaceous aerosol constituents in the lower stratosphere, *Geophys. Res. Lett.*, **36**, L12813, doi:10.1029/2009GL038735.
- Mather, T. A., D. M. Pyle, and A. G. Allen (2004b), Volcanic source for fixed nitrogen in Earth's early atmosphere, *Geology*, **32**, 905–908, doi:10.1130/G20679.1.
- McCormick, M. P., L. W. Thomason, and C. R. Trepte (1995), Atmospheric effects of the Mt. Pinatubo eruption, *Nature*, **373**(6513), 399–404, doi:10.1038/373399a0.
- Michelangeli, D. V., M. Allen, and Y. L. Yung (1991), Heterogeneous reactions with NaCl in the El Chichón volcanic aerosols, *Geophys. Res. Lett.*, **18**, 673–676.
- Neuman, J. A., L. G. Huey, T. B. Ryerson, and D. W. Fahey (1999), Study of inlet materials for sampling atmospheric nitric acid, *Environ. Sci. Technol.*, **33**, 1133–1136, doi:10.1021/es980767f.
- Neuman, J. A., et al. (2001), In situ measurements of  $\text{HNO}_3$ ,  $\text{NO}_y$ ,  $\text{NO}$  and  $\text{O}_3$  in the lower stratosphere and upper troposphere, *Atmos. Environ.*, **35**, 5789–5797, doi:10.1016/S1352-2310(01)00354-5.
- Popp, P. J., et al. (2007), Condensed-phase nitric acid in a tropical sub-visible cirrus cloud, *Geophys. Res. Lett.*, **34**, L24812, doi:10.1029/2007GL031832.
- Popp, P. J., et al. (2009), Stratospheric correlation between nitric acid and ozone, *J. Geophys. Res.*, **114**, D03305, doi:10.1029/2008JD010875.
- Reiner, T., and F. Arnold (1993), Laboratory flow reactor measurements of the reaction  $\text{SO}_3 + \text{H}_2\text{O} + \text{M} \rightarrow \text{H}_2\text{SO}_4 + \text{M}$ : Implications for gaseous  $\text{H}_2\text{SO}_4$  and aerosol formation in the plumes of jet aircraft, *Geophys. Res. Lett.*, **20**(23), 2659–2662, doi:10.1029/93GL02996.
- Reiner, T., and F. Arnold (1994), Laboratory investigations of gaseous sulfuric acid formation via  $\text{SO}_3 + \text{H}_2\text{O} + \text{M} \rightarrow \text{H}_2\text{SO}_4 + \text{M}$ : Measurement of the rate constant and product identification, *J. Chem. Phys.*, **101**, 7399–7407, doi:10.1063/1.468298.
- Rose, W. I., et al. (2006), Atmospheric chemistry of a 33–34 hour old volcanic cloud from Hekla Volcano (Iceland): Insights from direct sampling and the application of chemical box modeling, *J. Geophys. Res.*, **111**, D20206, doi:10.1029/2005JD006872.
- Schmale, J., et al. (2010), Aerosol layers from the 2008 eruptions of Mt. Okmok and Mt. Kasatochi: In situ UT/LS measurements of sulfate and organics over Europe, *J. Geophys. Res.*, **115**, D00L07, doi:10.1029/2009JD013628.
- Schneider, J., et al. (1999), The temporal evolution of the ratio  $\text{HNO}_3/\text{NO}_y$  in the Arctic lower stratosphere from January to March 1997, *Geophys. Res. Lett.*, **26**(8), 1125–1128, doi:10.1029/1999GL900184.
- Solomon, S. (1999), Stratospheric ozone depletion: A review of concepts and history, *Rev. Geophys.*, **37**, 275–316, doi:10.1029/1999RG900008.
- Solomon, S., R. W. Portmann, R. R. Garcia, W. Randel, F. Wu, R. Nagatani, J. Gleason, L. Thomason, L. R. Poole, and M. P. McCormick (1998), Ozone depletion at mid-latitudes: Coupling of volcanic aerosols and temperature variability to anthropogenic chlorine, *Geophys. Res. Lett.*, **25**, 1871–1874, doi:10.1029/98GL01293.
- Speidel, M., R. Nau, F. Arnold, H. Schlager, and A. Stohl (2007), Sulfur dioxide measurements in the lower, middle and upper troposphere: Deployment of an aircraft-based chemical ionization mass spectrometer with permanent in-flight calibration, *Atmos. Environ.*, **41**, 2427–2437, doi:10.1016/j.atmosenv.2006.07.047.
- Stockwell, W., and J. Calvert (1983), The mechanism of the  $\text{HO}-\text{SO}_2$  reaction, *Atmos. Environ.*, **17**(5), 2231–2235.
- Tabazadeh, A., and R. P. Turco (1993), Stratospheric chlorine injection by volcanic eruptions: HCl scavenging and implications for ozone, *Science*, **260**, 1082–1086.
- Textor, C., H. F. Graf, M. Herzog, and J. M. Oberhuber (2003), Injection of gases into the stratosphere by explosive volcanic eruptions, *J. Geophys. Res.*, **108**(D19), 4606, doi:10.1029/2002JD002987.
- Theys, N., M. Van Roozendaal, B. Dils, F. Hendrick, N. Hao, and M. De Mazière (2009), First satellite detection of volcanic bromine monoxide emission after the Kasatochi eruption, *Geophys. Res. Lett.*, **36**, L03809, doi:10.1029/2008GL036552.
- Tilmes, S., R. Garcia, R. Douglas, E. Kinnison, A. Gettelman, and P. Rasch (2009), Impact of geoengineered aerosols on the troposphere and stratosphere, *J. Geophys. Res.*, **114**, D12305, doi:10.1029/2008JD011420.
- Voigt, C., B. Kärcher, H. Schlager, C. Schiller, M. Krämer, M. de Reus, H. Vössing, S. Borrmann, and V. Mitev (2007), In-situ observations and modeling of small nitric acid-containing ice crystals, *Atmos. Chem. Phys.*, **7**, 3373–3383, doi:10.5194/acp-7-3373-2007.
- Voigt, C., et al. (2010), In-situ observations of young contrails - Overview and selected results from the CONCERT campaign, *Atmos. Chem. Phys.*, **10**, 1–18, doi:10.5194/acp-10-1-2010.
- Wernli, H., and H. C. Davies (1997), A Lagrangian-based analysis of extratropical cyclones. Part I: The method and some applications, *Q. J. R. Meteorol. Soc.*, **123**, 467–489, doi:10.1002/qj.49712353811.
- World Meteorological Organization (2007), Scientific assessment of ozone depletion: 2006, *Rep. 50*, 572 pp., Geneva, Switzerland.
- Woods, D. C., R. L. Chuan, and W. I. Rose (1985), Halite particles injected into the stratosphere by the 1982 El Chichón eruption, *Science*, **230**(4722), 170–172, doi:10.1126/science.230.4722.170.
- Ziereis, H., H. Schlager, P. Schulte, P. van Velthoven, and F. Slemr (2000), Distributions of  $\text{NO}$ ,  $\text{NO}_x$ , and  $\text{NO}_y$  in the upper troposphere and lower stratosphere between 28 and 61°N during POLINAT 2, *J. Geophys. Res.*, **105**, 3653–3664, doi:10.1029/1999JD900870.

Ziereis, H., et al. (2004), Uptake of reactive nitrogen on cirrus cloud particles during INCA, *Geophys. Res. Lett.*, *31*, L05115, doi:10.1029/2003GL018794.

Zentrum für Luft- und Raumfahrt, D-82234 Oberpfaffenhofen, Germany.  
(Tina.Jurkat@dlr.de)

J. Schmale and J. Schneider, Particle Chemistry, Max Planck Institute for Chemistry, D-55020 Mainz, Germany.

---

F. Arnold, H. Aufmhoff, A. Dörnbrack, T. Jurkat, M. Lichtenstern,  
H. Schlager, and C. Voigt, Institut für Physik der Atmosphäre, Deutsches